Simulations of a Protein Translocation Pore: SecY†

Shozeb Haider,‡ Benjamin A. Hall, and Mark S. P. Sansom*

Department of Biochemistry, University of Oxford, South Parks Road, Oxford OX1 3QU, U.K.

Received May 22, 2006; Revised Manuscript Received August 30, 2006

ABSTRACT: SecY is the central channel protein of the SecYEβ translocon, the structure of which has been determined by X-ray diffraction. Extended (15 ns) MD simulations of the isolated SecY protein in a phospholipid bilayer have been performed to explore the relationship between protein flexibility and the mechanisms of channel gating. In particular, principal components analysis of the simulation trajectory has been used to probe the intrinsic flexibility of the isolated SecY protein in the absence of the γ-subunit (SecE) clamp. Analysis and visualization of the principal eigenvectors support a "plug and clamshell" model of SecY channel gating. The simulation results also indicate that hydrophobic gating at the central pore ring prevents leakage of water and ions through the channel in the absence of a translocating peptide.

Molecular mechanisms of transport of solutes across membranes are a key topic in structural biology at present (*1*−*5*). A key step in the biosynthesis of many secreted and membrane proteins is their transport across the endoplasmic reticulum in eukaryotes or the plasma membrane in prokaryotes via a porelike protein known as the translocon (*6*). The translocon is a heterotrimeric complex formed of an α-subunit (SecY in eubacteria and archaea and Sec61α in mammals) which forms the pore, a γ-subunit (SecE in eubacteria and archaea and Sec61γ in mammals), and a β-subunit (SecG in eubacteria, Secβ in archaea, and Sec61β in mammals) (*7*−*9*). The α- and γ-subunits are conserved in sequence; the β-subunit is not. Cryo-EM studies of the *Escherichia coli* SecYEG complexed with a ribosome and a nascent polypeptide chain suggest channel formation by the opening of two linked SecY halves during polypeptide translocation (*10*).

The X-ray structure of the SecYEβ complex from the *Methanococcus jannaschii* has been determined at 3.5 Å resolution (*11*). The SecY complex consists of three separate polypeptides (SecYEβ) with a total of 12 transmembrane (TM)[1] helices. The SecY α-subunit (10 TM) forms the core of the channel. The β-subunit has a single TM helix. It is loosely connected to the α-subunit and is not required for channel function in vitro. SecE (or γ-subunit) contains a single long TM that is "clamped" around the α-subunit and is an essential gene. The two halves of the α-subunit (M1−5 and M6−10) are related to each other by 2-fold pseudosymmetry.

On the basis of analysis of the X-ray structure of the archeal SecYEβ complex (*11*), it has been suggested (*1*) that the two halves of the SecY molecule undergo a clamshell-like conformational change. This would open the pore laterally (between TM helices M2b and M7) to allow TM helices of a nascent membrane protein to enter the surrounding lipid bilayer. This contention is supported by cryo-electron microscopy of the *E. coli* SecYEG complex (*10*). It is also suggested that the transbilayer pore opens perpendicularly via displacement of a plug formed by the M2a segment. A hydrophobic gate [or "gasket" (*1*)] region is proposed to prevent leakage of water and/or ions.

Crystal structures provide a static (time and space average) picture of a protein. Molecular dynamics (MD) simulations (*12*) enable us to extend purely structural approaches to characterize the nanosecond time scale dynamics of membrane proteins (*13*, *14*). A couple of recent simulation studies have used steered (*15*) MD simulations to explore possible mechanisms of opening of the SecY pore (*16*, *17*). However, to fully understand the mechanism of protein transport, it is also important to determine the intrinsic flexibility of the SecY α-subunit. To do this, we have simulated the dynamics of the SecY protein in the absence of the other two components of the heterotrimeric complex. As in a recent application of this approach to a bacterial potassium channel [KirBac (*18*)], we then use essential dynamics (*19*) to describe the principal motions undertaken by the protein in these simulations. The simulation results appear to support the clamshell model (discussed above) of the mechanism of SecY-mediated protein transport.

METHODS

Simulation System. The coordinates of SecY, the α-subunit of the protein-conducting channel of *M. jannaschii*, were extracted from the Protein Data Bank (entry 1RHZ). All side chains were assumed to be in their standard ionization state. Residues 1 and 434−436 were absent from the X-ray structure and were not modeled in the structure used for

† This work was supported by a grant from the Wellcome Trust. B.A.H. is a Medical Research Council research student.

* To whom correspondence should be addressed. E-mail: mark.sansom@bioch.ox.ac.uk. Phone: +44-1865-275371. Fax: +44-1865-275273.

‡ Current address: The London School of Pharmacy, 29−39 Brunswick Square, Bloomsbury, London WC1N 1AX, U.K.

[1] Abbreviations: MD, molecular dynamics; PCA, principal components analysis; POPC, palmitoyloleoylphosphatidylcholine; SPC, single-point charge; TM, transmembrane.

10.1021/bi061013d CCC: $33.50
Published on Web 10/11/2006

simulations. The simulation system was prepared by embedding the SecY α-subunit in an equilibrated palmitoyloleoylphosphatidylcholine (POPC) bilayer. The protein was solvated using SPC waters (*20*) in a box with dimensions of 8 nm × 10 nm × 10 nm. Counterions were added to neutralize the system. The total system consisted of 53 780 atoms. Before running the simulations, we minimized the energy of the system using 1000 iterations of steepest descents. The system was then equilibrated for 0.25 ns, during which the non-hydrogen protein atoms were restrained using a force constant of 1000 kJ mol^{-1} nm^{-2}. During the equilibration, the lipids, water molecules, and ions were free to move. For the production run, all restraints were removed and the simulation was run for 15 ns.

Simulation Protocol. MD simulations were performed using GROMACS version 3.1.4 (*21*, *22*) (www.gromacs.org) employing a modified version of the GROMOS87 force field (*23*). The lipid parameters were based on those used in MD studies of dipalmitoylphosphatidylcholine bilayers (*24*, *25*). Berendsen coupling was employed (*26*) to maintain a constant temperature of 300 K and a constant isotropic pressure of 1 bar. Water, lipid, and protein were coupled separately to a temperature bath at 300 K, using a coupling constant of 0.1 ps. van der Waals interactions were modeled using 6-12 Lennard-Jones potentials with a 1.3 nm cutoff. Long-range electrostatics were calculated using the particle mesh Ewalds method (*27*, *28*), with a cutoff for the real space term of 1.2 nm. The LINCS algorithm was used to constrain bond lengths (*29*). The time step that was employed was 2 fs. Coordinates were saved every 10 ps for subsequent analysis.

Analysis was carried out using the GROMACS suite of packages plus local scripts. Structural diagrams were generated using VMD (*30*) or PyMol (www.pymol.org). Porcupine plots of eigenvectors were calculated using an approach derived from Tai et al. (*31*, *32*) as implemented in the Dynamite server (*33*). Secondary structure analysis employed DSSP (*34*).

Elastic Network Modeling. Elastic network models, using a protein topology based on the proximity of Cα atoms in a structure, were generated as described in, for example, ref *35*. All Cα atoms within a given cutoff of one another are linked by a "bond", with all bonds being assigned the same (arbitrary) force constant. Both one-dimensional (Gaussian network model) and three-dimensional (anisotropic network model) variants of the elastic model were employed (*36*, *37*). The cutoff used in the Gaussian network model was 0.7 nm; for the anisotropic model, it was 0.9 nm.

RESULTS

Conformational Drift and Flexibility. The resolution of the X-ray structure on which this simulation was based is 3.5 Å. Also, the simulation is of an isolated SecY subunit in a lipid bilayer (Figure 1). Before a more detailed analysis of the simulation was undertaken, it was therefore important to establish the overall conformational stability of the protein over the course of the simulation. The root-mean-square deviation (rmsd) of Cα atoms from the initial structure (Figure 2A) provides a simple overall measure of the conformational stability of the protein over the course of the simulation. After an initial increase over the first ~1 ns, the

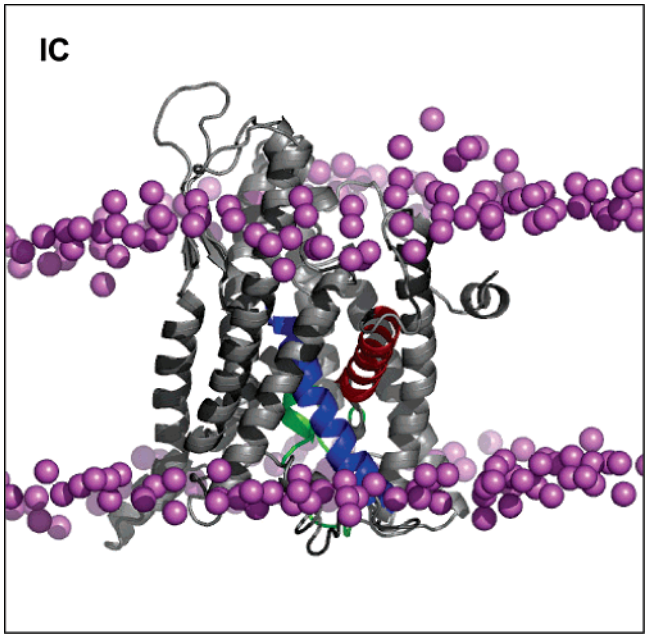

FIGURE 1: Simulation system, showing the SecY α-subunit embedded in a POPC bilayer. Transmembrane helices discussed in the text are color-coded: green for the plug, red for M2b, blue for M7, and gray for the remainder of SecY. The P atoms of the bilayer are colored lilac. The intracellular side (IC) of the protein is at the top of the figure.

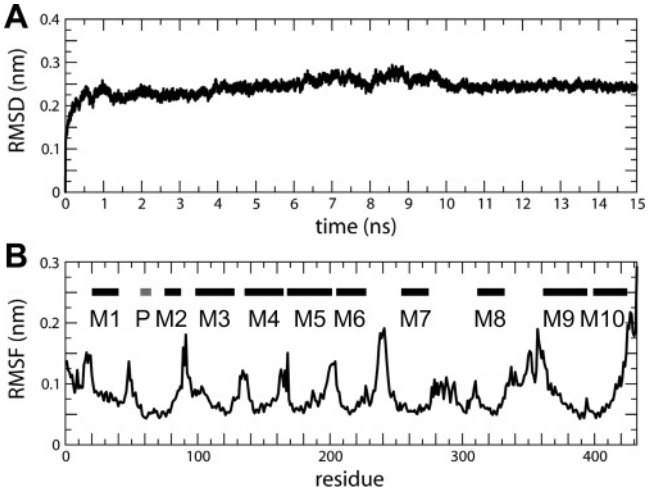

FIGURE 2: Conformation drift and fluctuations. (A) Structural drift of the protein during the simulation. The Cα atom root-mean-square deviation (rmsd) relative to the starting structure is plotted as a function of time. (B) Root-mean-square fluctuations (RMSF) of each Cα atom as a function of residue number. Residues that exhibit strong fluctuations correspond to the loop regions that connect the 10 helices (labeled M1−M10). The pore plug is labeled as P.

Cα rmsd is constant at 0.25 nm. This is typical of the behavior of many membrane proteins (*13*, *38*) and suggests that there is no overall drift in the SecY conformation, at least on a 10 ns time scale. We have also analyzed the secondary structure of SecY as a function of time (data not shown). There is a negligible loss of α-helicity within the TM helices. There is some limited change in secondary structure in the extended loop following M7. Thus, the simulation merits further analysis.

In terms of identifying the more flexible regions of the protein, we found it is informative to examine structural fluctuations. These can be measured as the root-mean-square

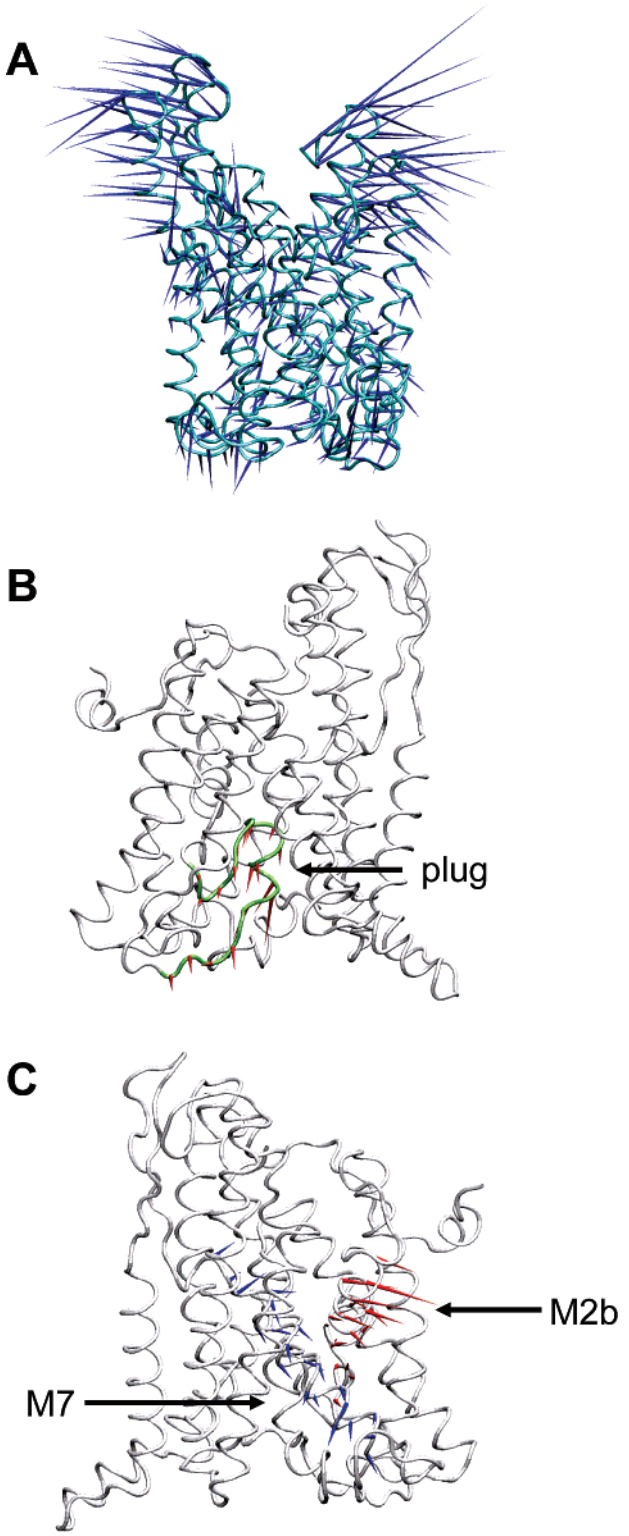

FIGURE 3: Principal components analysis (PCA) of protein motions. (A) Porcupine plot of the first eigenvector calculated from the covariance matrix. The SecY α-subunit is represented as a Cα trace. The arrows attached to each Cα atom indicate the eigenvector. (B) The first eigenvector of the pore plug (green) reveals a downward motion of the plug (red arrowheads). (C) The first eigenvector of the M2b and M7 helices exhibits a movement away from each, indicative of the opening of the lateral gate.

fluctuations (RMSF) from its time-averaged position of each Cα atom as a function of residue number (Figure 2B). The fluctuations are relatively small, with values of ~0.05 nm for the cores of the TM helices. Again, this is indicative of a conformationally stable protein. However, more detailed examination reveals some interesting patterns. As one would expect, the RMSF is largest at the N- and C-termini of the subunit. Also as expected, elevated RMSF values (>0.125 nm) reveal a greater degree of fluctuation in surface loops and bends and in the $\beta-$turn$-\beta$ motif between M6 and M7. Interestingly, the loops immediately before the plug and immediately after the M2b helix are relatively flexible, while that between the plug and the M2b helix is not. This suggests that the plug and M2b helix may move together.

Principal Motions. To characterize the dominant motions observed during the course of the simulation, we have carried out essential dynamics (principal components) analysis (PCA) (*19*, *39*). This requires calculation of the eigenvectors from the covariance matrix of a simulation. The trajectory may then be filtered on each of the different eigenvectors. Preliminary analysis revealed that the first three eigenvectors account for >50% of the protein motions, so we restricted our analysis to only these three eigenvectors. Helical bending at residue G30 in M1 and at G81 in M2b and swivel motions in M7 dominate the motions in all the three eigenvectors. Eigenvector 2 also reveals helical bending motion in M8. A helix bending motion at G214 in M6 is seen in eigenvector 3. Essential dynamics analysis also reveals considerable flexibility in the loop regions in the structure, mainly at glycine or proline residues. These results also suggest that there is a breakdown of the structural pseudosymmetry; i.e., a helix exhibits motions distinct from that of its pseudosymmetry-related partner during the course of the simulation.

The SecY subunit when viewed from the side resembles the letter X. Visualizing the principal motions using a porcupine plot (*32*) for eigenvector 1 indicates a simultaneous movement of the arms of X toward the equatorial position (Figure 3A), which might be expected to facilitate opening of the central pore of the protein. A more detailed inspection of the porcupine plot for eigenvector 1 in the region of the plug (Figure 3B) reveals a concerted "downward" movement (where the intracellular surface is defined as uppermost) away from the core of the protein. This is presumed to be facilitated by the two glycine residues at either side of the plug which may act as hinge points for the movement.

Elastic Network Model. One of the limitations of (all atom) MD simulations is the relatively short (10−100 ns) time scales that can be achieved for membrane proteins of any degree of complexity. In an analysis of the motions of proteins in such simulations, this raises the question of the extent to which such motions may be sampled within such a time window (*40*). One approach to this problem is to use more coarse-grained approaches to examine the motion of the protein (*41*). Such models include elastic network models (*35*−*37*, *42*), which can also be used within the framework of normal-mode analysis (*43*). The advantage of these models is that they allow one to focus on the low-frequency (i.e., long time scale) motions of a protein. The disadvantage is their lack of atomistic detail and, in the context of membrane proteins, the absence of any representation of the limit bilayer environment. It is therefore valuable to compare the results of elastic network model analysis with those from PCA of all atom MD simulations.

A Gaussian network model was used to calculate the magnitudes of the predicted motions and, hence, a profile of fluctuations (often expressed as crystallographic *B*-values)

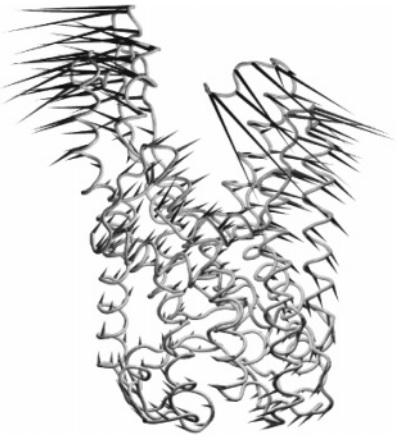

FIGURE 4: Elastic network model analysis of SecY motions. Porcupine plot of the first eigenvector calculated from the anisotropic elastic network model. As in Figure 3A (with which this may be compared), the arrows attached to each Cα atom indicate the eigenvector.

versus residue number which was compared with the RMSF versus residue number analysis (Figure 2B) discussed above. The correlation between the two approaches was very good (see the Supporting Information), suggesting that the MD simulation and elastic network model were revealing similar motions. In particular, the modes of the Gaussian network model bisect the protein along the axis of the pore, indicative of concerted opening−closing motions. Extending this analysis via an anisotropic elastic network model allows us to calculate and display the eigenvectors corresponding to the major low-frequency motions (Figure 4). These can be compared with the eigenvectors from the PCA of the MD simulations (Figure 3A). Encouragingly, the same overall pattern is observed in the elastic network model as in the MD simulations. This provides us with some confidence that the latter have sampled, albeit incompletely, the lower-frequency motions of SecY. One may examine the elastic network model-predicted motions in more detail, in particular with respect to the plug region of SecY. Although there are some differences from the MD simulations (which is not unexpected given the degree of coarse graining in the elastic network model), both analyses suggest a concerted motion of the plug away from the core of the SecY protein.

These results may also be compared with those of Mitra et al. (*10*), who combined normal-mode analysis with an elastic network model as part of their analysis of the structure of the *E. coli* translocon bound to a ribosome. Analysis of a "plug-less" model suggested an opening motion of two SecY halves. Thus, a number of different approaches, both atomistic and coarse-grained, seem to converge in their description of the motion of SecY. This suggests that further analysis of the key TM helix motions at the atomistic level afforded by MD simulations may be worthwhile.

TM2b−TM7 Interactions (Lateral Gate). When a secretory protein enters the translocon, the hydrophobic signal sequence is thought to be intercalated between M2b and M7 (*1*, *11*), which requires the "front" (i.e., the interface between the M3 and M2b helices on one side and the M7 and M8 helices on the other side) of the SecY subunit to open. The essential dynamics analysis (eigenvector 3) revealed helical bending motion at G214 in M6. It has been suggested that a small hinge motion of ∼15° between M5 and M6 would

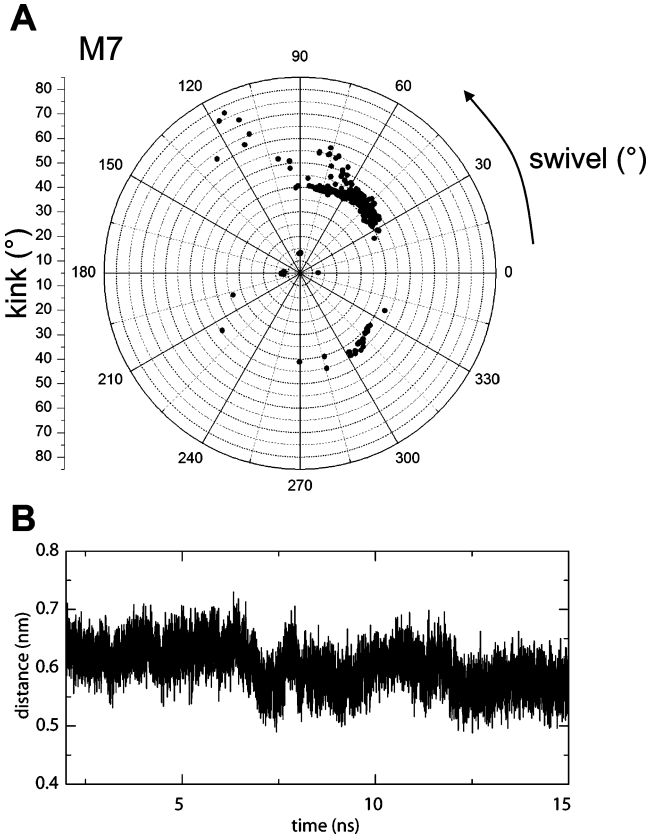

FIGURE 5: (A) Polar plot of the kink and swivel angles calculated from the first eigenvector of the M7 helix, saved every 0.1 ns over the course of the final 13 ns of the simulation run. (B) Minimum distance between helices M2b and M7 plotted as a function of time.

create a pore with dimensions of 15−20 Å front to back and 10−15 Å side to side, sufficient to allow insertion of a loop of a translocating peptide chain (*11*).

Transmembrane helices of nascent membrane proteins need to be expelled into the lipid bilayer laterally from the translocon protein. The interface between M2b and M7, and between M2b and M8, is the only place where this can happen since all other directions are blocked by the small subunits (SecE and γ) or obstructed by other segments of the SecY subunit. This region has been defined as a lateral gate (*1*). Essential dynamics analysis of TM2 and TM7 (Figure 3C) indicates the two helices move in different directions. A degree of helix bending at G81 is observed in M2b, whereas a clear swivel motion is observed for M7 (Figure 5A). Since M2b and M7 cross at an angle of ∼70°, any motions in opposing directions would tend to increase the distance between the two helices at the interface, thereby (partially) opening the lateral gate. Indeed, examination of the minimum distance between M2b and M7 as a function of time (Figure 5B) reveals fluctuations on an ∼5 ns time scale which support a degree of lability in the interaction between this pair of helices. Thus, although of course the lateral gate does not significantly open in this (relatively short) simulation (see below), the observed motions support a clamshell model in which M2b and M7 move relative to one another and also exhibit some degree of internal flexibility.

The center of the protopore in the SecY protein has a hydrophobic "pore ring" (*11*) (formed by the side chains of residues I75, V79, I170, I174, I260, and L406). In the

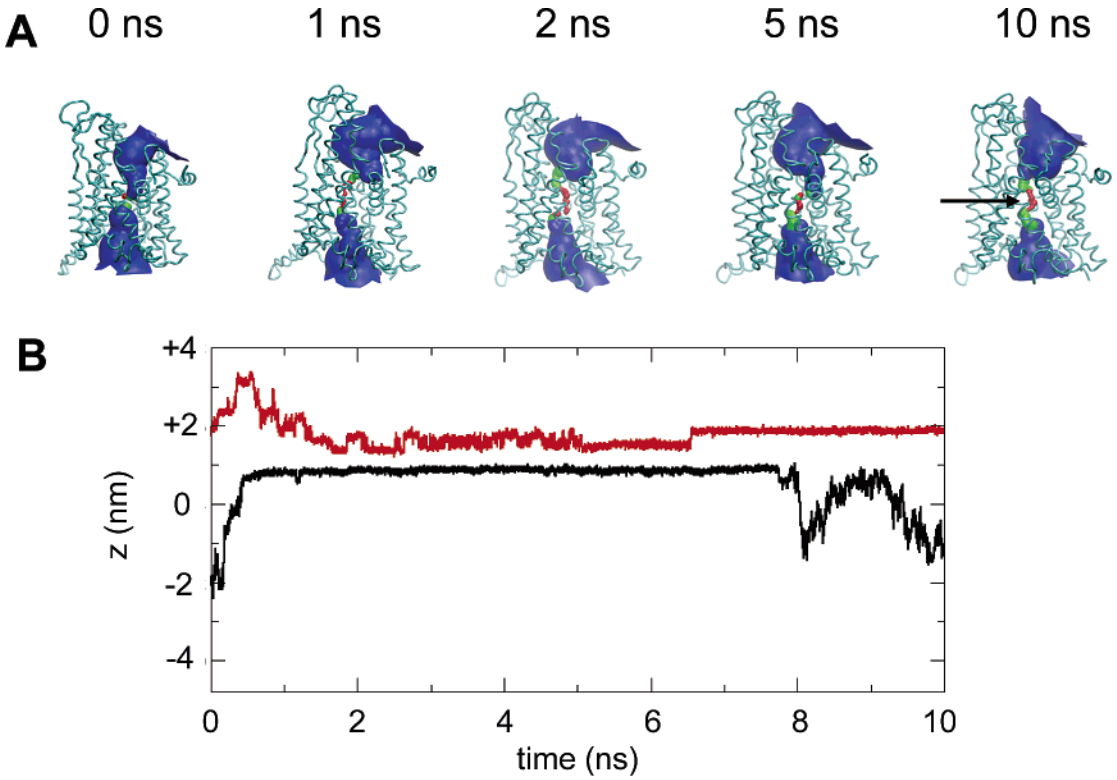

FIGURE 6: (A) Pore lining surfaces [calculated using HOLE (*60*)] of the SecY α-subunit generated from snapshots taken at different time intervals during the simulation. The pore ring which acts like a hydrophobic gate, narrowing the pore radius to ~0.14 nm, is indicated by the horizontal arrow. (B) Trajectories of two water molecules that approach the pore ring but are unable to cross it.

absence of a translocated peptide, this would be expected to remain in a functionally closed state. The pore radius at the ring region is ~0.14 nm. Simulations of simplified model pores (*44*−*46*) suggest a hydrophobic gate of these dimensions will be functionally closed. Calculation of the pore radius profile, using HOLE (*47*), and visualization of the inner surface of the pore (Figure 6A) reveal that the central constriction actually tightens during the first ~1 ns and then persists for the duration of the simulation. Examination of the trajectories of water molecules within the SecY protein (Figure 6B) reveals that although they may approach the pore ring from either side they do not cross, at least on an ~10 ns time scale. Thus, the pore ring remains closed throughout the simulation.

DISCUSSION

In this study, we performed an extended (15 ns) simulation of the isolated SecY α-subunit in a phospholipid bilayer. We simulated SecY in the absence of the β- and γ-subunits because we wished to explore its intrinsic flexibility. In particular, we wished to examine the dynamic behavior of SecY in the absence of the γ-subunit (SecE in archaea) which forms a clamp around the α-subunit. The intrinsic flexibility of SecY is likely to be of some biological importance. For example, a recent review of the structural biology of the translocon (*1*) discusses the functional importance of the flexibility of SecY. Indeed, one may view SecY as a gated pore for polypeptides which is regulated by interactions with other proteins (e.g., the other TM subunits, the nascent polypeptide chain, and/or intracellular components). In this context, the conformational dynamics of SecY underlying gating of the transbilayer pore clearly play a key role in translocon function. The main result of PCA of the SecY simulation is the suggestion of a concerted movement of the plug domain, in addition to evidence of flexibility of helices M2 and M7 which may form the lateral gate. This is consistent with the gating mechanisms of SecY suggested on the basis of examination of the X-ray structure of the closed state of the pore.

Transport of polypeptides through the SecY pore occurs on an ~1 s time scale (*48*). Clearly, an ~15 ns time scale simulation therefore will not directly reveal substantial conformational changes underlying pore gating. However, via principal components analysis of an extended equilibrium simulation of the SecY closed state, we can determine the principal eigenvectors which may indicate elements of the dynamic flexibility of the protein that are consistent with the proposed unplugging (M2a) and clamshell (M2b/M7) conformational change. However, one should exercise caution. In essence, by adopting such an approach, we are examining motions dictated by the local energy landscape of the closed state, in an attempt to infer pathways of conformational change that lead to the open state(s). Supporting this general approach to analysis of conformational flexibility are a number of analyses of bacterial potassium channels. Thus, extended MD simulations of an isolated TM domain combined with PCA have been used to explore gating mechanisms in KirBac (*18*). Related approaches using either normal-mode analysis (*49*) or elastic network models (*50*) have been applied to KcsA and other bacterial potassium channels. All of these methods support gating models consistent with available X-ray diffraction data (*51*). Thus, one may have some degree of confidence in the overall approach to exploring the conformational dynamics of the closed state to reveal clues concerning gating mechanisms.

We have also compared the results of elastic network model analysis with those from the atomistic MD simulations. Both levels of modeling support the plug and clamshell model of SecY opening, although there are of course (given the different granularity of the two models) some differences in the details. Similar results in terms of SecY opening via a clamshell-like mechanism were suggested by normal-mode analysis of an elastic network model of a plug-less SecY (*10*) and have been obtained via a distance geometry-based method using the Dynamite server (http://dynamite.biop.ox.ac.uk/dynamite) (*33*) (B. A. Hall and M. S. P. Sansom, unpublished results). Thus, we may have some degree of confidence in the sampling of SecY motions by the MD simulations.

The results of the current simulation also inform our understanding of the hydrophobic gate as formed by the pore ring region of SecY. This remains closed throughout the simulation. Indeed, HOLE analysis of the pore suggests that if anything at the end of the simulation the gate is a little more tightly closed than in the X-ray structure. By tracking water molecules close to this gate, we observed that although a water molecule (bottom trace in Figure 6B) was able to move past the M2a plug, no water molecule was able to cross the hydrophobic gate. This is consistent with current theoretical views of hydrophobic gating (*45*, *46*).

It is interesting to compare our study to two recent simulation studies of the translocon, both of which focused on the SecYEβ complex rather than the SecY protein per se. Schulten and colleagues (*16*) used steered MD simulations of SecYE in a phospholipid bilayer, in which they pulled simple hydrophobic polypeptides through the pore. Although the time scale of pulling (1−5 ns total) is somewhat faster than the in vivo transport rate (~1 s), these studies revealed that the plug domain could be displaced and suggested that water molecules may be able to move through the pore alongside the steered peptide. In a simulation in an implicit membrane model (*17*), Tian and Andricioaei used an "expanding sphere" approach [similar to that previously used to drive open the pore of KcsA (*52*)] to perturb the SecYEβ structure toward an open state. Both of these studies also yielded results consistent with the plug and clamshell model of SecY gating. However, it should be stressed that our study is the first to use an extended equilibrium (i.e., unperturbed) simulation to explore the intrinsic flexibility of the closed state.

It is important also to explore the relationship of these simulations to experimental studies. The simulations appear to be consistent with the gating model proposed on the basis of the X-ray structure of the translocon monomer. This model is also supported by more recent cryo-electron microscopic images of the translocon bound to a ribosome (*10*). In particular, normal-mode fitting of the closed SecYE X-ray structure to the electron microscopy density of the open pore favors the clamshell model of conformational change in SecY. This is of considerable interest in the context of the two-state model of membrane protein folding (*53*) and its later modifications (*54*) which suggest that TM helices are independent folding domains. Recent experimental studies have probed the dependence of translocon-mediated TM helix insertion on peptide sequence (*55*). By combining simulations of translocon−helix interactions (*16*) with simulations of helix−bilayer interactions (*56*), one may be able to more fully understand how the clamshell SecY pore gating model facilitates insertion of a helix into lipid bilayers and thus contributes to membrane protein folding (*57*).

There are clearly limitations to the current simulation study, some of which are discussed above. Perhaps the major ones are the absence of the β- and γ-subunits, combined with the time scale of the simulations relative to the process of peptide translocation. The latter will not be able to be addressed by direct atomistic simulation in the immediate future. However, it is conceivable that recent developments in coarse-grained simulations of membrane proteins (*58*) and in elastic network models (*35*, *36*, *59*) in simulating longer time scale conformational changes in proteins will allow us to simulate larger length scale and longer time scale events underlying protein translocation. It would also be of interest to apply such methods to compare the competing proposals for how the translocon dimer functions, i.e., to compare the "back-to-back" model (*11*) in which each translocon monomer forms an independent pore with the "front-to-front" model (*10*) in which some degree of functional interaction between the two translocon pores may occur.

ACKNOWLEDGMENT

Our thanks to all of our colleagues for their interest in this work, especially Alessandro Grottesi.

SUPPORTING INFORMATION AVAILABLE

Comparison of a RMSF profile and a calculated *B*-value profile from a Gaussian network model analysis of SecY. This material is available free of charge via the Internet at http://pubs.acs.org.

REFERENCES

1. Clemons, W. M., Ménétret, J.-F., Akey, C. W., and Rapoport, T. A. (2004) Structural insight into the protein translocation channel, *Curr. Opin. Struct. Biol. 14*, 390−396.
2. Lemieux, M. J., Huang, Y., and Wang, D. N. (2004) The structural basis of substrate translocation by the *Escherichia coli* glycerol-3-phosphate transporter: A member of the major facilitator superfamily, *Curr. Opin. Struct. Biol. 14*, 405−412.
3. Abramson, J., Kaback, H. R., and Iwata, S. (2004) Structural comparison of lactose permease and the glycerol-3-phosphate antiporter: Members of the major facilitator superfamily, *Curr. Opin. Struct. Biol. 14*, 413−419.
4. Pebay-Peyroula, E., and Brandolin, G. (2004) Nucleotide exchange in mitochondria: Insight at a molecular level, *Curr. Opin. Struct. Biol. 14*, 420−425.
5. Locher, K. P. (2004) Structure and mechanism of ABC transporters, *Curr. Opin. Struct. Biol. 14*, 426−431.
6. Driessen, A. J., Manting, E. H., and van der Does, C. (2001) The structural basis of protein targeting and translocation in bacteria, *Nat. Struct. Biol. 8*, 492−498.
7. Gorlich, D., Hartmann, E., Prehn, S., and Rapoport, T. A. (1992) A protein of the endoplasmic reticulum involved early in polypeptide translocation, *Nature 357*, 47−52.
8. Gorlich, D., Prehn, S., Hartmann, E., Kalies, K. U., and Rapoport, T. A. (1992) A mammalian homolog of SEC61p and SECYp is associated with ribosomes and nascent polypeptides during translocation, *Cell 71*, 489−503.
9. Hanada, M., Nishiyama, K. I., Mizushima, S., and Tokuda, H. (1994) Reconstitution of an efficient protein translocation machinery comprising SecA and the three membrane proteins, SecY, SecE, and SecG, *J. Biol. Chem. 269*, 23625−23631.
10. Mitra, K., Schaffitzel, C., Shaikh, T., Tama, F., Jenni, S., Brooks, C. L., Ban, N., and Frank, J. (2005) Structure of the *E. coli* protein-conducting channel bound to a translating ribosome, *Nature 438*, 318−324.

11. van den Berg, B., Clemons, W. M., Collinson, I., Modis, Y., Hartmann, E., Harrison, S. C., and Rapoport, T. A. (2004) X-ray structure of a protein-conducting channel, *Nature 427*, 36−44.
12. Karplus, M. J., and McCammon, J. A. (2002) Molecular dynamics simulations of biomolecules, *Nat. Struct. Biol. 9*, 646−652.
13. Ash, W. L., Zlomislic, M. R., Oloo, E. O., and Tieleman, D. P. (2004) Computer simulations of membrane proteins, *Biochim. Biophys. Acta 1666*, 158−189.
14. Gumbart, J., Wang, Y., Aksimentiev, A., Tajkhorshid, E., and Schulten, K. (2005) Molecular dynamics simulations of proteins in lipid bilayers, *Curr. Opin. Struct. Biol. 15*, 423−431.
15. Isralewitz, B., Baudry, J., Gullingsrud, J., Kosztin, D., and Schulten, K. (2001) Steered molecular dynamics investigations of protein function, *J. Mol. Graphics Modell. 19*, 13−25.
16. Gumbart, J., and Schulten, K. (2006) Molecular dynamics studies of the archael translocon, *Biophys. J. 90*, 2356−2367.
17. Tian, P., and Andricioaei, I. (2006) Size, motion, and function of the SecY translocon revealed by molecular dynamics simulations with virtual probes, *Biophys. J. 90*, 2718−2730.
18. Grottesi, A., Domene, C., and Sansom, M. S. P. (2005) Conformational dynamics of M2 helices in KirBac channels: Helix flexibility in relation to gating via molecular dynamics simulations, *Biochemistry 44*, 14586−14594.
19. Amadei, A., Linssen, A. B. M., and Berendsen, H. J. C. (1993) Essential dynamics of proteins, *Proteins: Struct., Funct., Genet. 17*, 412−425.
20. Berendsen, H. J. C., Postma, J. P. M., van Gunsteren, W. F., and Hermans, J. (1981) *Intermolecular Forces*, Reidel, Dordrecht, The Netherlands.
21. Berendsen, H. J. C., van der Spoel, D., and van Drunen, R. (1995) GROMACS: A message-passing parallel molecular dynamics implementation, *Comp. Phys. Commun. 95*, 43−56.
22. Lindahl, E., Hess, B., and van der Spoel, D. (2001) GROMACS 3.0: A package for molecular simulation and trajectory analysis, *J. Mol. Model. 7*, 306−317.
23. van Gunsteren, W. F., and Berendsen, H. J. C. (1987) *Gromos-87 manual*, Biomos BV, Groningen, The Netherlands.
24. Berger, O., Edholm, O., and Jahnig, F. (1997) Molecular dynamics simulations of a fluid bilayer of dipalmitoylphosphatidycholine at full hydration, constant pressure and constant temperature, *Biophys. J. 72*, 2002−2013.
25. Marrink, S. J., Berger, O., Tieleman, D. P., and Jahnig, F. (1998) Adhesion forces of lipids in a phospholipid membrane studied by molecular dynamics simulations, *Biophys. J. 74*, 931−943.
26. Berendsen, H. J. C., Postma, J. P. M., van Gunsteren, W. F., DiNola, A., and Haak, J. R. (1984) Molecular dynamics with coupling to an external bath, *J. Chem. Phys. 81*, 3684−3690.
27. Darden, T., York, D., and Pedersen, L. (1993) Particle mesh Ewald: An N.log(N) method for Ewald sums in large systems, *J. Chem. Phys. 98*, 10089−10092.
28. Essmann, U., Perera, L., Berkowitz, M. L., Darden, T., Lee, H., and Pedersen, L. G. (1995) A smooth particle mesh Ewald method, *J. Chem. Phys. 103*, 8577−8593.
29. Hess, B., Bekker, H., Berendsen, H. J. C., and Fraaije, J. G. E. M. (1997) LINCS: A linear constraint solver for molecular simulations, *J. Comput. Chem. 18*, 1463−1472.
30. Humphrey, W., Dalke, A., and Schulten, K. (1996) VMD: Visual Molecular Dynamics, *J. Mol. Graphics 14*, 33−38.
31. Tai, K., Shen, T., Henchman, R. H., Bourne, Y., Marchot, P., and McCammon, J. A. (2002) Mechanism of acetylcholinesterase inhibition by fasciculin: A 5-ns molecular dynamics simulation, *J. Am. Chem. Soc. 124*, 6153−6161.
32. Tai, K., Shen, T., Börjesson, U., Philippopoulos, M., and McCammon, J. A. (2001) Analysis of a 10-ns molecular dynamics simulation of mouse acetylcholinesterase, *Biophys. J. 81*, 715−724.
33. Barrett, C. P., Hall, B. A., and Noble, M. E. M. (2004) Dynamite: A simple way to gain insight into protein motions, *Acta Crystallogr. D60*, 2280−2287.
34. Kabsch, W., and Sander, C. (1983) Dictionary of protein secondary structure: Pattern-recognition of hydrogen-bonded and geometrical features, *Biopolymers 22*, 2577−2637.
35. Bahar, I., Atilgan, A. R., and Erman, B. (1997) Direct evaluation of thermal fluctuations in proteins using a single-parameter harmonic potential, *Folding Des. 2*, 173−181.
36. Atilgan, A. R., Durell, S. R., Jernigan, R. L., Demirel, M. C., Keskin, O., and Bahar, I. (2001) Anisotropy of fluctuation dynamics of proteins with an elastic network model, *Biophys. J. 80*, 505−515.
37. Eyal, E., Yang, L., and Bahar, I. (2006) Anisotropic Network Model: Systematic evaluation and a new web interface, *Bioinformatics* (in press).
38. Law, R. J., Capener, C., Baaden, M., Bond, P. J., Campbell, J., Patargias, G., Arinaminpathy, Y., and Sansom, M. S. P. (2005) Membrane protein structure quality in molecular dynamics simulation, *J. Mol. Graphics Modell.* **24**, 157−165.
39. Garcia, A. E. (1992) Large-amplitude nonlinear motions in proteins, *Phys. Rev. Lett. 68*, 2696−2699.
40. Faraldo-Gómez, J. D., Forrest, L. R., Baaden, M., Bond, P. J., Domene, C., Patargias, G., Cuthbertson, J., and Sansom, M. S. P. (2004) Conformational sampling and dynamics of membrane proteins from 10-nanosecond computer simulations, *Proteins: Struct., Funct., Bioinf. 57*, 783−791.
41. Tozzini, V. (2005) Coarse-grained models for proteins, *Curr. Opin. Struct. Biol. 15*, 144−150.
42. Yang, L. W., Liu, X., Jursa, C. J., Holliman, M., Rader, A. J., Karimi, H. A., and Bahar, I. (2005) iGNM: A database of protein functional motions based on Gaussian Network Model, *Bioinformatics 21*, 2978−2987.
43. Tirion, M. M. (1996) Large amplitude elastic motions in proteins from a single-parameter, atomic analysis, *Phys. Rev. Lett. 77*, 1905−1908.
44. Beckstein, O., Biggin, P. C., and Sansom, M. S. P. (2001) A hydrophobic gating mechanism for nanopores, *J. Phys. Chem. B 105*, 12902−12905.
45. Beckstein, O., and Sansom, M. S. P. (2003) Liquid−vapor oscillations of water in hydrophobic nanopores, *Proc. Natl. Acad. Sci. U.S.A. 100*, 7063−7068.
46. Beckstein, O., Tai, K., and Sansom, M. S. P. (2004) Not ions alone: Barriers to ion permeation in nanopores and channels, *J. Am. Chem. Soc. 126*, 14694−14695.
47. Smart, O. S., Goodfellow, J. M., and Wallace, B. A. (1993) The pore dimensions of gramicidin A, *Biophys. J. 65*, 2455−2460.
48. White, S. H., and von Heijne, G. (2004) The machinery of membrane protein assembly. *Curr. Opin. Struct. Biol. 14*, 397−404.
49. Shen, Y. F., Kong, Y. F., and Ma, J. P. (2002) Intrinsic flexibility and gating mechanism of the potassium channel KcsA, *Proc. Natl. Acad. Sci. U.S.A. 99*, 1949−1953.
50. Shrivastava, I. H., and Bahar, I. (2006) Common mechanism of pore opening shared by five different potassium channels, *Biophys. J. 90*, 3929−3940.
51. Jiang, Y., Lee, A., Chen, J., Cadene, M., Chait, B. T., and MacKinnon, R. (2002) The open pore conformation of potassium channels, *Nature 417*, 523−526.
52. Biggin, P. C., and Sansom, M. S. P. (2002) Open-state models of a potassium channel. *Biophys. J. 83*, 1867−1876.
53. Popot, J. L., and Engelman, D. M. (1990) Membrane protein folding and oligomerization: The two-state model, *Biochemistry 29*, 4031−4037.
54. Engelman, D. M., Chen, Y., Chin, C., Curran, R., Dixon, A. M., Dupuy, A., Lee, A., Lehnert, U., Mathews, E., Reshetnyak, Y., Senes, A., and Popot, J. L. (2003) Membrane protein folding: Beyond the two stage model, *FEBS Lett. 555*, 122−125.
55. Hessa, T., Kim, H., Bihlmaier, K., Lundin, C., Boekel, J., Andersson, H., Nilsson, I., White, S. H., and von Heijne, G. (2005) Recognition of transmembrane helices by the endoplasmic reticulum translocon, *Nature 433*, 377−381.
56. Freites, J. A., Tobias, D. J., von Heijne, G., and White, S. H. (2005) Interface connections of a transmembrane voltage sensor, *Proc. Natl. Acad. Sci. U.S.A. 102*, 15059−15064.
57. Bowie, J. U. (2005) Solving the membrane protein folding problem, *Nature 438*, 581−589.
58. Bond, P. J., and Sansom, M. S. P. (2006) Insertion and assembly of membrane proteins via simulation, *J. Am. Chem. Soc. 128*, 2697−2704.
59. Keskin, O., Jernigan, R. L., and Bahar, I. (2000) Proteins with similar architecture exhibit similar large-scale dynamic behavior, *Biophys. J. 78*, 2093−2106.
60. Smart, O. S., Neduvelil, J. G., Wang, X., Wallace, B. A., and Sansom, M. S. P. (1996) HOLE: A program for the analysis of the pore dimensions of ion channel structural models, *J. Mol. Graphics 14*, 354−360.

BI061013D